Multiscale analysis of turbulence-flame interaction based on measurements in premixed flames

Chantriaux, François; Quenouille, Théo; Doan, Nguyen Anh Khoa; Swaminathan, Nedunchezhian; Hardalupas, Yannis; Taylor, A. M.K.P.

DOI
10.1016/j.combustflame.2022.111982

Publication date
2022

Document Version
Final published version

Published in
Combustion and Flame

Combustion and Flame 239 (2022) 111982

Contents lists available at ScienceDirect

Combustion and Flame

journal homepage: www.elsevier.com/locate/combustflame

Multiscale analysis of turbulence-flame interaction based on measurements in premixed flames

François Chantriaux[a], Théo Quenouille[b], Nguyen Anh Khoa Doan[c], Nedunchezhian Swaminathan[d], Yannis Hardalupas[e], AMKP Taylor[e,*]

[a] Ecole Polytechnique, Palaiseau, France
[b] ENSTA Paris, Institut Polytechnique de Paris, Palaiseau, France
[c] Faculty of Aerospace Engineering, Technical University of Delft, Kluyverweg 1, 2629 HS Delft, The Netherlands
[d] Department of Engineering, University of Cambridge, Trumpington Street, Cambridge CB2 1PZ, United Kingdom
[e] Thermofluids Division, Department of Mechanical Engineering, Imperial College London, London SW7 2BX, United Kingdom

ARTICLE INFO

Article history:
Received 23 June 2021
Revised 3 January 2022
Accepted 4 January 2022
Available online 1 February 2022

Keywords:
Stereo particle image velocimetry
Laser induced planar fluorescence
Turbulent premixed flame
Flame-turbulence interaction
Multiscale decomposition
Flame tangential strain rate

ABSTRACT

Multi-scale analysis of turbulence-flame interaction is performed using experimental data sets from three methane- and propane-fired premixed, turbulent V-flames, at an approach flow turbulent Reynolds number of 450 and a ratio of r.m.s. fluctuating velocity from the mean to laminar flame speed of between 2.1 and 3.0, straddling the border between corrugated flamelets and thin reaction zone in the Borghi-Peters diagram. The measurements were made in the plane of a single laser sheet using stereo particle image velocimetry SPIV and planar laser-induced fluorescence to measure three orthogonal components of velocity and flame OH. Methods to approximate the remaining, unmeasured, out of plane derivatives are described. The instantaneous SPIV images were bandpass filtered at user-specified characteristic length scales L_ω and L_s (for vorticity and strain rate, respectively) resulting in instantaneous bandpass-filtered velocity fields, $\underline{u}_b^{L_\omega}$ and $\underline{u}_b^{L_s}$, which were further analysed to give the bandpass filtered vorticity field, $\underline{\omega}^{L_\omega} = \nabla \times \underline{u}_b^{L_\omega}$, the strain-rate field, $e_{ij}^{L_s}$, and the tangential strain rate field $a_T^{L_s}$. This work quantifies two aspects of turbulence-flame interaction. The first aspect is that of the flame interaction of eddies of size L_s on the turbulence, as found by the statistics of the alignment of vorticity with strain rate. We find that vortical eddies with scale about $L_\omega = 2\delta_{th}$ (where δ_{th} is the flame thickness) are stretched by L_s structures which are larger than about 2 L_ω, with this factor broadly true also for vortical eddies of scales $L_\omega = 4\delta_{th}$ and $L_\omega = 6\delta_{th}$. Within the limitations of the data set, these findings are consistent with those in the literature on reacting and non-reacting flows, suggesting that the premixed flame has had little influence on the vortex stretching mechanism. The second aspect of turbulence-flame interaction examined is that of flame surface-averaged tangential strain rate imparted by eddies. Eddies with length scales L_s smaller than 3 or $4\delta_{th}$ are likely to have the strongest individual contribution but eddies of this length scale and smaller may contribute only about 1/5th of the total tangential strain rate. This is to be compared with the value of 10% that has been reported in the literature based on analysis of DNS predictions of premixed flames at turbulent Reynolds numbers up to 110. Eddies with length scale L_s larger than about $20\delta_{th}$ contribute a negligible amount to the total tangential strain rate. We have found no evidence that the Lewis number up to about 1.8 has an observable effect, but this may reflect the limitations of the current experiment. In the context of large eddy simulations (LES) of premixed combustion, these results are preliminary experimental evidence supporting the suggestion that resolving turbulence scales down to a few multiples of δ_{th} might be adequate to capture much of the flame straining caused by turbulence.

1. Introduction

Bray [1] laid out, in a paper published more than four decades ago, an exposition of "The interaction between turbulence and combustion". A seminal result was to show that if there exists a progress variable for the global combustion reaction[1], in the limit of large fluctuations as exist in most turbulent premixed flames, and at high turbulence Reynolds number, the mean reaction rate

* Corresponding author.
E-mail address: a.m.taylor@imperial.ac.uk (A. Taylor).

[1] Thus excluding compressible flows, flows with heat losses, or flows with non-unity Lewis number.

https://doi.org/10.1016/j.combustflame.2022.111982
0010-2180/

in combustion is related to the scalar dissipation rate

$$\overline{\dot{\omega}} = K_2 \overline{\chi} \tag{1}$$

$$\overline{\chi}_i \equiv 2\overline{\rho D \frac{\partial c''}{\partial x_k} \frac{\partial c''}{\partial x_k}} \tag{2}$$

where $\overline{\dot{\omega}}$ is the time-averaged chemical reaction rate; $K_2 = 1/(2c_m - 1)$ where c_m is determined from the ratio of two successive moments of the probability density function of c, which is a reaction progress variable; $\overline{\chi}$ is the time-averaged scalar dissipation rate of c; and the double prime denotes fluctuation from the Favre-average. The limit of large fluctuations implies that the local mixture is overwhelmingly made up of burnt and unburnt gas packets, separated by (in this limit) reaction zones of negligible thickness. This further can be shown to imply that the Damkoehler number is large, meaning that the rate of combustion is controlled by turbulent mixing rather than by chemical kinetics. If a wrinkled laminar flamelet analysis is also appropriate, all species concentrations as well as intermediates can be related to the mean local temperature from calculations of the undisturbed laminar flame. As the characteristic fluctuating integral velocity scale becomes comparable to, or exceeds, the laminar planar unstretched flame speed, turbulence interacts with, and distorts, the laminar flamelet structure by straining and curvature effects. The current contribution concerns itself, experimentally, with this interaction between combustion and turbulence [2] in premixed flames, manifested as the 'distortion' associated with the wrinkling and straining of the flame which are caused, respectively, by the vorticity- and strain-dominated structures in turbulence.

Wrinkling and stretching produce flame stretch, as quantified by fractional changes in its elemental surface area δA [3]:

$$\kappa = \frac{1}{\delta A}\frac{\mathrm{d}\delta A}{\mathrm{d}t} = \left(\delta_{ij} - n_i n_j\right) e_{ij} + s_d \frac{\partial n_i}{\partial x_i} = a_T + s_d K_m \tag{3}$$

where δ_{ij} is the Kronecker symbol; $\underline{n} = -\nabla c/|\nabla c|$ is unit normal to the flame surface pointing towards the fresh gases, found from the reaction progress variable c; n_i is the component of $\underline{n}$ in the x_i direction; $e_{ij} = 0.5(\partial u_i/\partial x_j + \partial u_j/\partial x_i)$ is the strain tensor with u_i being the turbulent velocity component in the direction i; and $s_d = (Dc/Dt)/|\nabla c|$ is the displacement speed, [4]. The last equation on the right summarises the effect of stretch in terms of tangential strain rate, a_T, and curvature, $K_m = \nabla \cdot \underline{n}$, which arise from straining and wrinkling. Qualitatively, low to moderate stretch rate creates active flame surface: in contrast, too high a stretch rate might result in the flame being quenched.

The flame stretch appears in several approaches for turbulent combustion modelling and calculation, including in the 'flame surface density' description as a source for flame surface area [5,6], where the surface averaged stretch can be negative [7–9], and in LES for the thickened flame model [10–12], and in the 'G equation' approach [12]. For both Reynolds Averaged Navier-Stokes (RANS) [13,14] and LES [10,11] calculations of premixed combustion, proposals include the 'strained flamelets' approach and the use of an 'efficiency (correction) function'. These approaches work well for RANS calculations and, for LES calculations which resolve most of the dynamic scales, there may be no need to try to account for the effect of sub-grid eddies, because these eddies may be too weak to stretch the flame. [14], by modelling the tangential strain rate acting on flame surfaces in RANS, introduced this efficiency function. It was derived by combining turbulence theory and DNS results to account for the fact that the strain generated by the vortex (*i.e.* the rate of strain $(r/\delta_{th}) \cdot (v_r/r)$ induced by a vortex dipole of characteristic velocity and length scale v_r and r) is not entirely converted into effective flame stretch (*i.e.* $(1/A)(\mathrm{d}A/\mathrm{d}t)$). This function mainly

Nomenclature

a_T	Tangential strain rate
c	Reaction progress variable
c_m	A constant determined from the ratio of moments of the probability density function of c
D	Diffusivity of c
D_f	Fractal dimension, $D_f = -log(4)/log(R_l)$
Da	Damkoehler number
e_{ij}	Strain rate tensor $0.5(\partial u_i/\partial x_j + \partial u_j/\partial x_i)$
K_m	Flame curvature, $\nabla \cdot \underline{n}$
K_2	A constant $K_2 = 1/(2c_m - 1)$
Ka	Karlovitz number, the ratio of the chemical timescale to the Kolmogorov timescale
L_G	Gibson scale s_L^3/ϵ
L_R	Empirically determined minimum vortex size that wrinkles the flame
L_s^+	L_s/δ_{th}
L_ω	characteristic lengthscale chosen to bandpass filter the vorticity field
L_s	Characteristic lengthscale chosen to bandpass filter the rate of strain field
L	Characteristic length scale of bandpass filter
Le	Lewis number
$\underline{n}$	$-\nabla c/\|\nabla c\|$ is the flame normal vector
n_i	Component of $\underline{n}$ in the x_i direction
$\underline{n}$	The unit normal to the flame surface pointing towards the fresh gases
Re_T	Reynolds number based on turbulence
s_d	$Dc/Dt/\|\nabla c\|$ is the displacement speed
s_L	Flame propagation speed in the normal direction
t	time
u_1'	Characteristic fluctuating velocity; or axial r.m.s. fluctuating velocity around the mean measured by hot wire anemometry
u_i	Components of velocity vector
x_i	Cartesian coordinate system. Axis of the stabilising wire runs along the x_3 coordinate
δ_{th}	Laminar flame thickness based on the maximum temperature gradient
δA	Change of elemental flame area
δ_{ij}	Kronecker symbol
ϵ	Dissipation rate of turbulent kinetic energy
η	Kolmogorov microscale
κ	Flame stretch $= \frac{1}{\delta A}\frac{\mathrm{d}\delta A}{\mathrm{d}t}$
Λ	Integral length scale of the turbulent flow
λ	Taylor microscale
ν	Kinematic viscosity
ρ	Density
τ	Heat release parameter $\frac{T_b - T_u}{T_u}$ with T_b, T_u the temperature of the burned and unburned gases respectively
ϕ	Equivalence ratio
$\overline{\chi}$	Scalar dissipation rate
$\widehat{\psi}\left(L_s^+\right)$	Fractional contribution of eddies at the normalised bandpass filtered scale $\left(L_s^+\right)$ to the tangential strain rate, equation 4
$\psi\left(L_s^+\right)$	Surface-averaged value of tangential strain rate at the normalised bandpass filtered scale $\left(L_s^+\right)$, equation 5
ψ^*	Cumulative distribution of $\widehat{\psi}$
$\overline{\dot{\omega}}$	Time-averaged chemical reaction rate
$\underline{\omega}$	vorticity vector

reduces or eliminates the influence of the smallest turbulent motions (*i.e.* smaller than a size of the order of few flame thicknesses), which are found to be unable to wrinkle the flame front. This work was subsequently extended to LES, and further developed by Colin et al. [10], Charlette et al. [11], Bougrine et al. [15], Thiesset et al. [16]. On the basis of experiments, however, Steinberg and Driscoll [17] and Steinberg and Driscoll [18] concluded that not only was an interaction between a vortex pair and a planar flame surface comparatively rare, but also that the straining and wrinkling of the flame surface were not well characterised by the vortical structures. Instead, straining and wrinkling were generally caused by large groups of multiply curved and intertwined structures. In addition, they found that stretch-efficiency functions developed from simplified vortex-flame interactions substantially over-predict the measurements.

Be that as it may, the efficiency function correctly highlights what might be expected, namely that length scales larger than the flame thickness can stretch the flame more 'efficiently' than do small scales. In this context, Poinsot et al. [19] and Roberts et al. [20] concluded that the Kolmogorov scales had lower efficiency for flame stretching ; Lipatnikov et al. [21], Nada et al. [22] in contrast, suggested that this scale produced the highest stretch. Nada et al. [22] and Yenerdag et al. [23] suggested the Taylor timescale to be an appropriate scaling factor for the tangential strain rate but thermo-diffusive instabilities may affect the flame-turbulence interaction in these hydrogen- air flames. Such contradictory views raised two questions, namely (1) what is the smallest turbulence scale imparting significant flame stretch and (2) what is the implication for modelling of the filtered reaction rate in LES? As already stated, the flame wrinkling and straining are caused, respectively, by the vorticity- and strain- dominated structures in turbulence. In turn, the vortical structures are produced by the vortex stretching mechanism in turbulence and hence the influence of the turbulence-flame interaction on this mechanism also becomes of interest.

To answer these questions, Doan et al. [24] analysed five premixed flames generated by Direct Numerical Simulation (DNS), spanning from the corrugated-flamelet to the thin reaction zones in the regime diagram of Peters. They analysed the instantaneous velocity field by educing turbulent eddies of various sizes using the multiscale analysis called bandpass filtering [25] which filters out scales smaller than the specified one, and larger ones less sharply: the analysis is briefly described in Section 2.4.1. This allowed the construction of filtered rate-of-strain fields, $e_{ij}^{L_s}$, and filtered vorticity fields, $\underline{\omega}^{L_\omega} = \nabla \times \underline{u}_b^{L_\omega}$ (where L_ω and L_s refer to the characteristic length scales chosen to filter the vorticity and strain rate fields). The intensity of vorticity of the velocity field which is bandpassed at length L_ω is quantified in terms of the filtered enstrophy field $0.5|\underline{\omega}^{L_\omega}|^2$.

In terms of flame wrinkling, the results show that downstream of the flame there are fewer small scale vortical structures (in terms of the enstrophy structures at length scale L_ω comparable to the flame thickness structures), confirming that a flame dampens turbulence, as might be expected. Nevertheless, the influence of the flame on the mechanism of vortex stretching, and the role of relative eddy sizes on this mechanism, were not unduly influenced by the presence of chemical reactions and heat release. These conclusions were established by investigating the vortex stretching mechanism which produces enstrophy at scale L_ω due to straining structures at scale L_s, namely $\omega_i^{L_\omega}\omega_j^{L_\omega}e_{ij}^{L_s} = |\underline{\omega}^{L_\omega}|^2\left(\alpha^{L_s}\cos^2\theta_\alpha + \beta^{L_s}\cos^2\theta_\beta + \gamma^{L_s}\cos^2\theta_\gamma\right)$ where α^{L_s}, β^{L_s} and γ^{L_s} are the principal components of $e_{ij}^{L_s}$ with $\alpha^{L_s} > \beta^{L_s} > \gamma^{L_s}$ and the θ_i are the corresponding angles between the vorticity vector and these principal components. The alignment between the vorticity vector, $\underline{\omega}$, and the principal components of strain rate tensor was similar to the non-reacting flow results in [25], namely that there is a preferential alignment of $\underline{\omega}$ with α from eddies larger than the vortical structure and the alignment with β is approached when L_s is less than or equal to L_ω. Specifically, the peak probability of $0.98 \leq |\cos\theta_\alpha| \leq 1$ as a function of L_s/L_ω occurred between 3 and 4 for the flames, implying that the vortical structure is stretched mostly by structures 3 to 4 times bigger than itself.

In terms of tangential strain rate, their results suggested that eddies in the range $3 \leq L_s/\delta_{th} \leq 17$ have substantial effect on flame straining, while eddies smaller than 3 δ_{th}, and eddies larger than 17 δ_{th}, contributed less than 20% and 10% to the total tangential strain rate respectively. This was established by investigating $\widehat{\psi}\left(L_s^+\right)$, the fractional contribution of eddies of scale $L_s^+ = L_s/\delta_{th}$ (the normalised bandpass filtered scale) to the tangential strain rate $a_T^{L_s} = (\delta_{ij} - n_i n_j)e_{ij}^{L_s}$:

$$\widehat{\psi}\left(L_s^+\right) = \psi\left(L_s^+\right)/\psi_{int} \tag{4}$$

where $\psi\left(L_s^+\right)$ is a surface-averaged value at the scale L_s^+

$$\psi\left(L_s^+\right) = \left\langle |\nabla c| a_T^{L_s^+}\right\rangle / \langle |\nabla c|\rangle \tag{5}$$

and $\psi_{int} = \int_0^\infty \psi \, \mathrm{d}L_s^+$ is the surface-averaged contribution coming from all scales in the flow. The corresponding cumulative distribution is $\psi^* = \int_0^{L_s} \widehat{\psi} \, dL_s^+$.

Eq. (4) leads to the definition of two cut-off length scales: ℓ_p^+ corresponds to the peak surface-averaged tangential strain rate, $\widehat{\psi}$, and ℓ_{10}^+ corresponds to $\psi^* = 0.1$. The latter identifies the eddy size below which the contribution to the total tangential strain rate experienced by the flame is 10%. Other cut-off scales exist in the literature, including the Gibson length scale, $L_G = s_L^3/\epsilon$ where ϵ is the dissipation rate of turbulent kinetic energy, and L_R which is an empirically determined minimum vortex size that wrinkles the flame [20] (as further discussed below in Eq. (14)). Doan et al. [24] concluded, by comparing these four length scales, that the range of eddies having weak influence on straining the flame is larger than originally thought. The significance is that this implies that resolving turbulence scales down to a few multiples of δ_{th} would be enough to capture most of the flame straining caused by turbulence. These scales can be captured by the LES equations and implies that additional modelling may not be required for sub-grid scale flame stretching. The results of [24] relate to cases for u'/s_L, the ratio of characteristic fluctuating velocity to laminar flame speed, up to about 11 and for Re_T, turbulence Reynolds number, up to about 110. They concluded that investigation should be extended to combustion at higher Re_T and to flows with shear, which are common in practical combustors.

In this contribution, we seek to extend the work of [24] by examining an experiment data set, rather than DNS, at high Re_T and including the effect of Lewis number. The preceding DNS analysis has been well controlled in every aspect, thereby opening the way for experimental observations to be explained with greater confidence: in addition, experimental data can be generated at substantially higher turbulent Reynolds number than is possible with DNS. There are differing opinions on the effect of increasing levels of turbulence (is there a higher impact of smaller scales of turbulence? Or change in the combustion regime in the Borghi-Peters diagram, for example?) so it is interesting to see if there is any consistency in the results. The experimental data used for this analysis are described in Section 2 and the bandpass filtering technique is discussed in Section 3. The results are presented and discussed in Section 4, and conclusions are summarised in the final section.

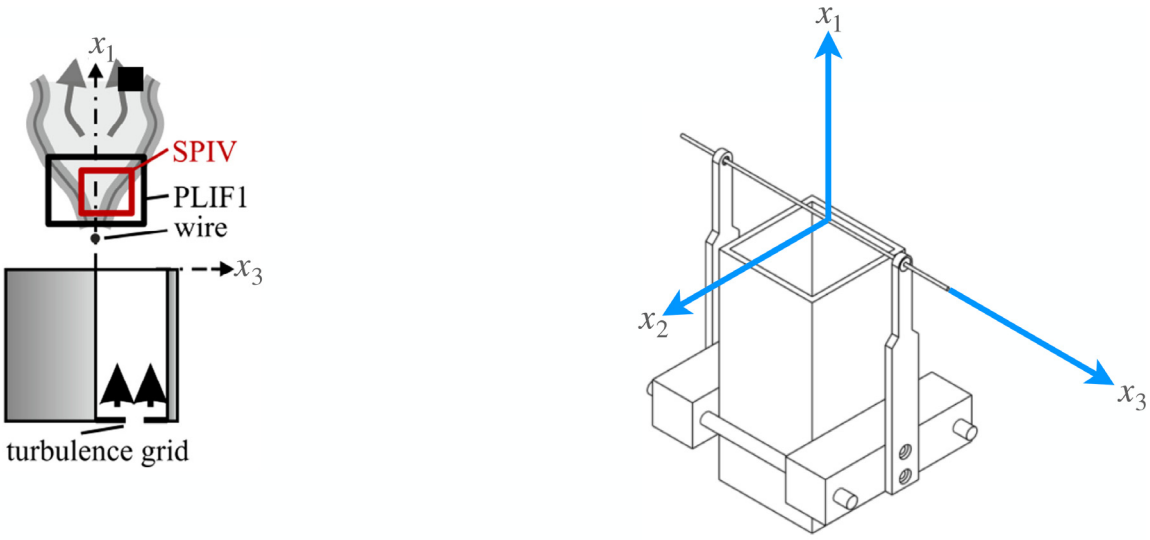

Fig. 1. Schematic of the burner, wire flame holder and field of view of the PLIF (grey) and SPIV (red) instruments with the definition of the coordinate system (based on [27]). (For interpretation of the references to colour in this figure legend, the reader is referred to the web version of this article.)

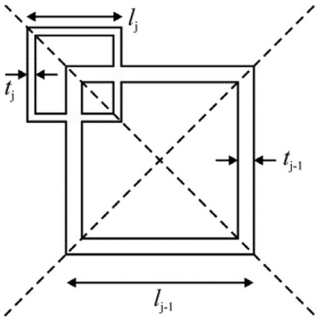

(a) parametrized structure

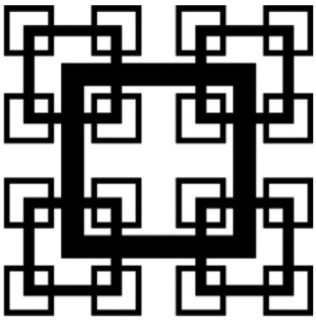

(b) grid used in this experiment

N	3
D_f	2
σ	0.37
l_0	$38.88mm$
R_l	0.5
t_0	$4.22mm$
R_t	0.43

(c) design parameters

Fig. 2. Fractal grid for generation of turbulence. D_f is the fractal dimension $D_f = -log(4)/log(R_l)$; N is the number of fractal iterations; $R_t = t_i/t_{i-1}$ and $R_l = l_i/l_{i-1}$ are the fractal iteration ratios for turbulence grid bar thickness, t, and length, l; σ is the blockage ratio.

2. Experiments and instrumentation

2.1. Burner

Three experiments were conducted on premixed, turbulent, V-flames stabilised on a 1.02 mm diameter stainless-steel wire, mounted 10 mm downstream of a square duct's exit plane: Fig. 1 shows elevation and isometric views. Sponfeldner [26,27] describes the experiments in detail. The premixed reactant stream, fuel (methane or propane) and air, flowed through the square duct (600 x 62 x 62 mm) which contained a series of flow-conditioning elements and, lastly, a fractal 'square grid' (designated 'FG3' in [26]), Figure 2, to initiate a turbulent flow 100 mm upstream of the exit. Fractal grids [28] produce substantially larger turbulence intensities than regular grids and create vigorous turbulence near the flame, appropriate for the study of turbulence-flame interaction. A comprehensive description of the details of the evolution of the turbulence downstream of the grid can be found [29].

Measurements from a single-component hot-wire anemometer gave the axial mean and r.m.s. fluctuating velocities, $\overline{u}_1$, u'_1. Computation of the temporal autocorrelation of the x_1 (streamwise) velocity gave the integral length scale, Λ, the Taylor microscale, λ, and the turbulent Reynolds number, Re_T, listed in Table 1. Eq. (6) provides the means to calculate the Kolmogorov length scale, η, assuming homogeneous, isotropic turbulence (with ν being the kinematic viscosity):

Table 1
Isothermal turbulence properties at the flame stabilising wire and flame parameters ([26] .

Property	Value	Property	Value
$\overline{u}$ (m/s)	5.5	u' (m/s)	0.75
Λ (mm)	9	Re_T	450
λ (mm)	3.6	η (mm)	0.12

$$\eta = \left(\frac{\nu^2\lambda^2}{30u_1'^2}\right)^{1/4} \tag{6}$$

Table 2 summarises the properties of the three flames. Flame 1 was a methane-air flame with an equivalence ratio of 0.8. Flames 2 and 3 were selected to change both the laminar burning velocity, s_L and Lewis number, Le, variables which might have an effect of interest in this investigation. To do so, the equivalence ratio of Flame 2 was increased to $\phi = 0.9$ and for Flame 3 propane was used instead of methane. Flame 3 also had the largest laminar burning velocity while having the same heat release parameter, τ, as Flame 2. The magnitudes of the Damkoehler Da and Karlovitz Ka numbers, together with values of the integral length scale Λ, the thermal flame thicknesses, δ_{th}, the characteristic turbulent velocity,

Table 2
Properties of the three investigated flames. Details of calculation of δ_{th}, s_L, τ and Le in [27] .

Flame	Fuel	ϕ	δ_{th}, mm	s_L, m/s	τ	Le	Da	Ka	Λ/δ_{th}	u'_1/s_L
1	CH_4	0.8	0.55	0.25	5.8	1.01	5.45	0.83	16.4	3.0
2	CH_4	0.9	0.48	0.33	6.3	1.01	8.25	0.49	18.8	2.3
3	C_3H_8	0.9	0.45	0.36	6.4	1.83	9.6	0.42	20.0	2.1

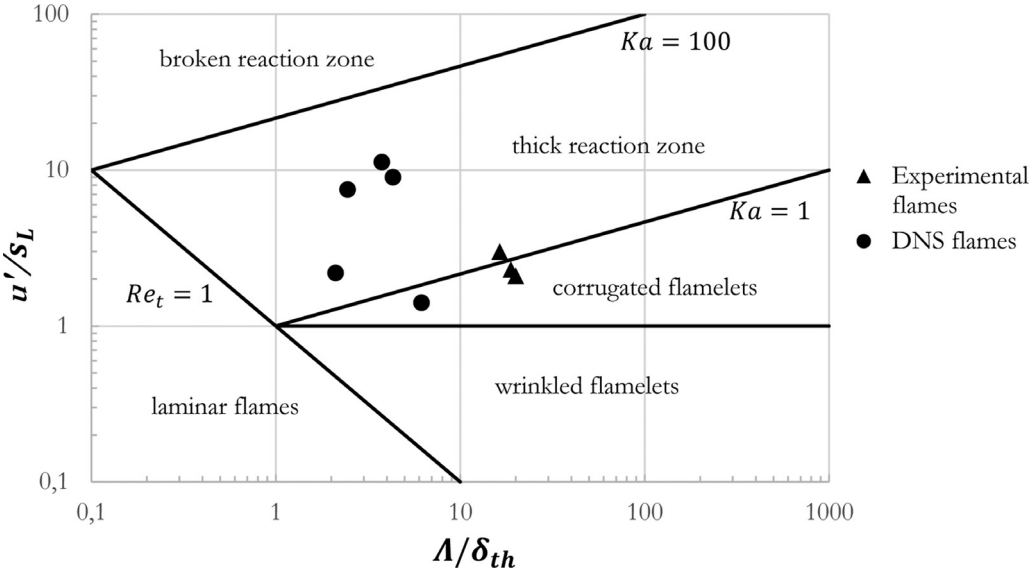

Fig. 3. Borghi-Peters diagram.

Table 3
SPIV parameters [27] .

Parameter	Value
Stereo-angle	90 deg.
Camera resolution HSS8	1024 x 1024 (x_1 x x_2)
Camera resolution HSS6	1024 x 992 (x_1 x x_2)
Field of view	25 mm x 21 mm
Vector spacing	0.39 mm

u'_1, and the laminar flame speeds s_L, placed the flames close to the boundary between the corrugated flamelet and thin reaction zone regimes in the Borghi/Peters diagram Fig. 3. Flames 1, 2 and 3 are represented respectively by open circles: the flames studied in the work by Doan et al. [24] are represented by blocked black squares. For convenience, Table 2 summarises the values of Λ/δ_{th} and u'/s_L.

2.2. Stereoscopic particle image velocimetry

Stereoscopic particle image velocimetry (SPIV, details in [27]) measured the aerodynamic field in an x_1, x_2 plane. The principle features of the system are given in Table 3. Such measurements yielded four components only of the strain-rate tensor: this two-dimensional information of the strain-rate field is a tolerable estimate of the nine-component strain-rate tensor, e_{ij}, because the investigated flow field was also predominantly two-dimensional and close to homogeneous in the x_3 direction. This was because out-of-laser-sheet derivatives of velocity are small compared to the derivatives within the measurement plane. The spacing of the velocity vectors was 0.39 mm. The field of view was about 25mm by 22mm. Vector validation, and a 3 x 3 Gaussian smoothing filter, were applied to the vector fields for the subsequent analysis.[27] quotes errors of 6.5% for the in-plane velocity components and 10.5% for the through-plane velocity.

2.3. Planar laser induced fluorescence

Planar laser-induced fluorescence imaging of the OH radical (OH-PLIF, details in [27]) was applied simultaneously in an imaging plane that was co-planar with that of the SPIV instrument to identify the reaction zone location of the flame in the SPIV measurement plane. OH-PLIF images from flames in the thin flame regime permit the extraction of the flame front location by the identification of the high gradient in the OH fluorescence signal between the unburnt and burnt gases. The images were corrected for background noise, for inhomogeneities in the imaging system sensitivity, and for non-uniform laser illumination. The corrected images were smoothed with a Gaussian convolution filter (1.6mm kernel size) and a nonlinear diffusion filter (contrast parameter 0.05, kernel 4 pixels, 25 iterations) to reduce noise and enhance flame contours.

In this work, an additional offset of the PLIF coordinates was applied until a satisfactory alignment is achieved, by about 1.6mm (40 pixels), which was found to give the best result in all the sampled frames.

2.4. Data processing

The experimental data provided the u_1, u_2 and u_3 components of the velocity (respectively along x_1, x_2 and x_3 axis).

2.4.1. Multiscale analysis method

In the analysis to be performed in the next few sections, the multiscale analysis method used is the bandpass filtering method presented in [24,25] which allows us to educe the effect of eddies associated a particular 'characteristic' length scale L. A summary of the steps to execute the method are described next. First, the original velocity field, $\underline{u}$, is Fourier transformed and the Fourier coefficients, denoted $\widehat{\underline{u}}$ where $\widehat{\cdot\cdot}$ indicates the Fourier-transformed quantity, are multiplied by a bandpass transfer function, $T_b(h) =$

$\sqrt{8/L}h^2\exp(h^2)$ with $h = kL/2$ where $k = |\underline{k}|$ is the magnitude of the wavenumber. The spatial filter extends between about L and $4L$, with a peak at $\sqrt{5}L$ and results in an instantaneous, spatially bandpass filtered velocity field, denoted $\underline{u}_b^L$, appropriate to the chosen length scale L. Second, the resulting Fourier coefficients, denoted $\widehat{\underline{u}}_b^L$, are then inverse Fourier-transformed to obtain the bandpass filtered velocity field, $\underline{u}_L^b$ which represents the effect of eddies which have a typical length scale L. Finally, using this bandpass-filtered velocity field, further quantities of interest can then be computed given a specified length scale L, such as the vorticity $\underline{\omega}^{L_\omega} = \nabla \times \underline{u}_b^{L_\omega}$, strain-rate $e_{ij}^{L_s}$ fields, and the tangential strain rate $a_T^{L_s}$. However, given the planar nature of the measurements, the latter quantities can be evaluated in a given x_1, x_2 plane only. Hence, the spatial derivatives in the x_3 direction remain unknown : $\frac{\partial u_1}{\partial x_3}$, $\frac{\partial u_2}{\partial x_3}$, $\frac{\partial u_3}{\partial x_3}$. This is also the case for $\frac{\partial c}{\partial x_3}$.

Several authors have discussed how to infer three-dimensional statistics from two-dimensional data in the context of the flame surface density ([30][31];[32];, among others). [31] advised linking the fluctuations in both transverse directions rather than relating the fluctuations in one transverse-, and the downstream-, directions as initially proposed by Halter et al. [30]. Hawkes et al. [32] assumes the case of isotropic scalar fields and turbulence and discusses the estimation of the tangential strain rate in the flame surface density balance equation, arriving at a factor of 2 as the conversion factor by which the two dimensional (measured) tangential strain should be multiplied to obtain the three-dimensional result.

2.5. Out-of-plane velocity derivatives approximation

The approach to the problem of inferring three-dimensional statistics from two-dimensional data adopted in this work was to analyse a DNS data set of a similar turbulent V-flame, to investigate approximate values for the missing experimental components. The DNS data set, being fully three dimensional, had all velocity and c spatial derivatives available through finite differencing and thereby allowed for a self-consistent analysis of velocity and scalar gradients. This approach allows us to deduce *qualitative* information which are consistent with many previous studies

The DNS data used here was generated by Dunstan et al. [33]: the simulation was fully compressible, three dimensional and the turbulence intensity $u_1'/s_L = 2$ is similar to that of the experimental flames presented in Table 2. The domain was a cube of side $12.77mm$, meshed with a 512^3 points uniform grid. The spatial step was $\approx 0.025mm$.

2.5.1. $\partial u_3/\partial x_3$ Approximation

The adopted method was, with reference to the DNS data, to find two different approximations for reacting and non-reacting regions, to study the behaviour of $\frac{\partial u_3}{\partial x_3}$ relatively to the full '3D' divergence of the flow and to the divergence of the flow based on the measured velocities restricted to the two dimensions (2D) of the laser sheet. It can be shown that [34]:

$$div(\underline{u}) = \frac{\tau}{1+\tau c}\frac{Dc}{Dt} \tag{7}$$

where $\tau = \frac{T_b - T_u}{T_u}$ with T_b, T_u being the temperatures of the burnt products and unburnt reactants respectively. This equation, known as the dilatation equation, allows one to deduce the dilatation rate using the scalar field information at a given instant, which is often the case while post-processing saved DNS data, since $Dc/Dt = (\dot{\omega}_c + \nabla \cdot \rho\mathcal{D}\nabla c)/\rho$ (note that tomography with *high-speed* laser diagnostics will also allow the deduction of Dc/Dt directly and thus $\nabla \cdot \underline{u}$ can be estimated). From the definition of dilatation, we would have

$$\frac{\partial u_3}{\partial x_3} = div(\underline{u}) - \frac{\partial u_1}{\partial x_1} - \frac{\partial u_2}{\partial x_2} \tag{8}$$

and we introduce the quantity $div_{2D}(\underline{u})$

$$div_{2D}(\underline{u}) \equiv \frac{\partial u_1}{\partial x_1} + \frac{\partial u_2}{\partial x_2} \tag{9}$$

The separation of reacting from non-reacting regions was based on the spatial gradient of the reaction progress variable, $|\underline{grad}\ c| \leq 1mm^{-1}$ for non-reacting regions and $|\underline{grad}\ c| > 1mm^{-1}$ for reacting regions. This results in the partition of the PIV window (Fig. 4). The sensitivity of the choice of the threshold level to discriminate between reactions and non-reacting regions has been investigated by halving, and doubling, the threshold gradient. We find that there is little influence.

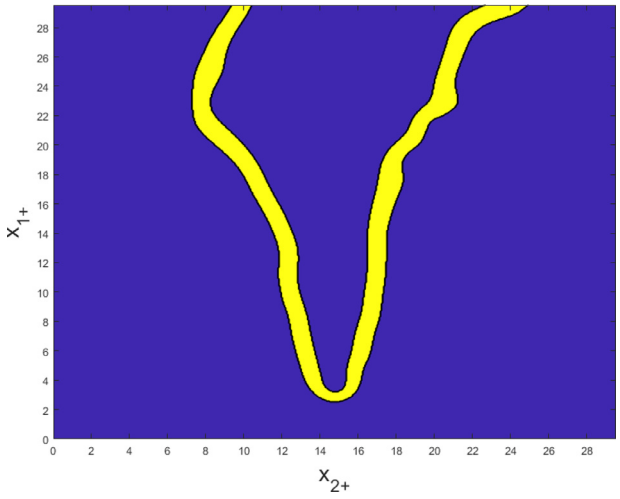

Fig. 4. Partition of the PIV window: figure depicts the x_1, x_2 plane (numbers on ordinate and abscissa are distances normalised by δ_{th}). Non-reacting regions in blue, reacting regions in yellow. (For interpretation of the references to colour in this figure legend, the reader is referred to the web version of this article.)

- *Non-reacting regions*

Figs. 5 and 7 show that the 3D divergence is very close to zero for a large majority of grid points (the error being associated with the method of separating the reacting from the non-reacting regions of the flow). This is confirmed by Fig. 9 which shows that the zero divergence assumption is a good approximation : $\frac{\partial u_3}{\partial x_3} \approx -\frac{\partial u_1}{\partial x_1} - \frac{\partial u_2}{\partial x_2}$. This assumption was used when processing experimental data for non-reacting regions.

- *Reacting regions*

Figs. 6 and 8 show that in combustion, as expected, the divergence increases considerably towards positive values and Fig. 10 confirms that the 'no divergence' assumption is invalid. However, importantly, Figure 6 shows that the measured $div_{2D}(\underline{u})$ is a tolerable approximation to $div_{3D}(\underline{u})$. Hence, the contribution of $\frac{\partial u_3}{\partial x_3}$ to $div_{2D}(\underline{u})$ is here neglected in reacting regions and $\frac{\partial u_3}{\partial x_3} = 0$ was the assumption adopted for reacting regions.

2.5.2. $\partial u_1/\partial x_3$ and $\partial u_2/\partial x_3$ approximation

The method for these two terms, once again in relation to the DNS data, is to use random distributions, on the basis that we expect - in this flow which is a close approximation to being two-dimensional in the mean in the x_1, x_2 plane - neither $\partial u_1/\partial x_3$ nor $\partial u_2/\partial x_3$ to be correlated with other terms in the rate of strain tensor. This in turn is owing to there being, in the mean, no shear stress in the x_1, x_3 plane. This method comes down to using two

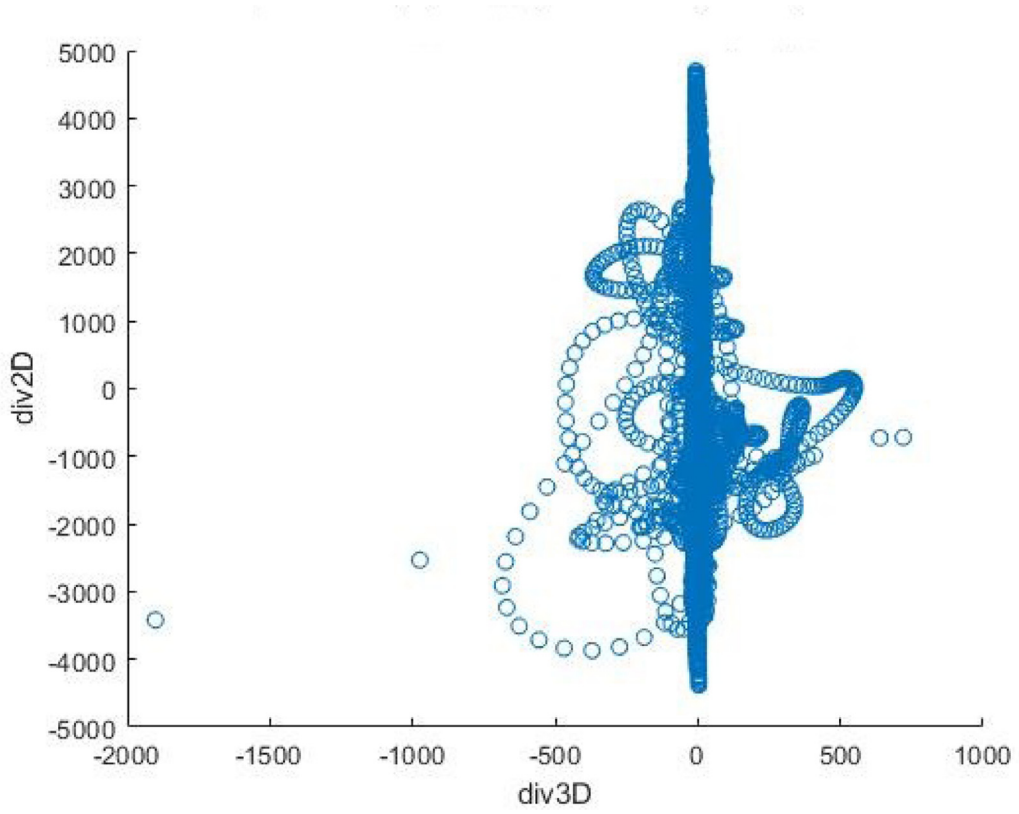

Fig. 5. div_{2D} against div_{3D} in non-reacting regions.

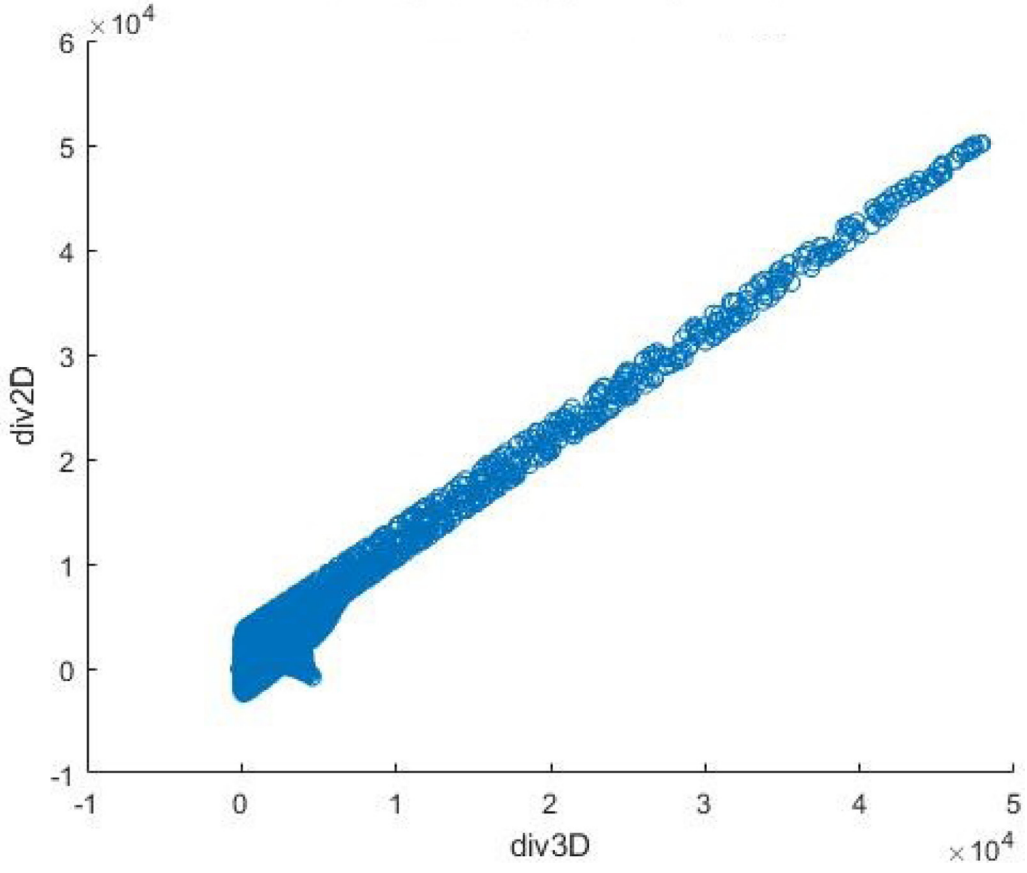

Fig. 6. div_{2D} against div_{3D} in reacting regions.

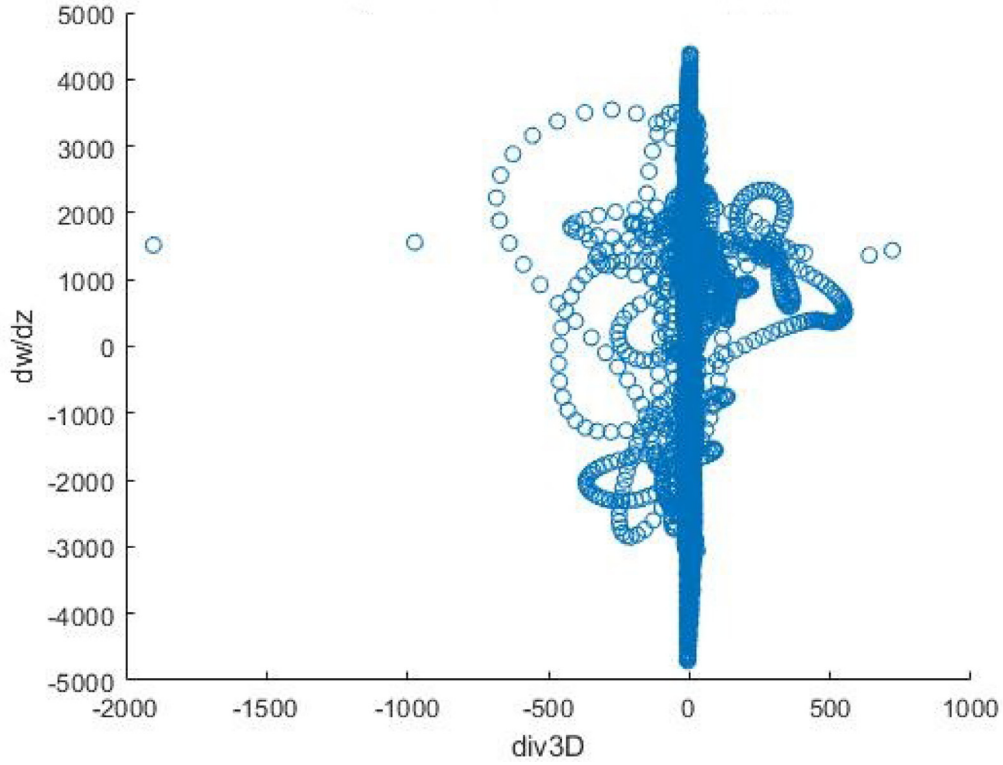

Fig. 7. $\frac{\partial u_3}{\partial x_3}$ against div_{3D} in non-reacting regions.

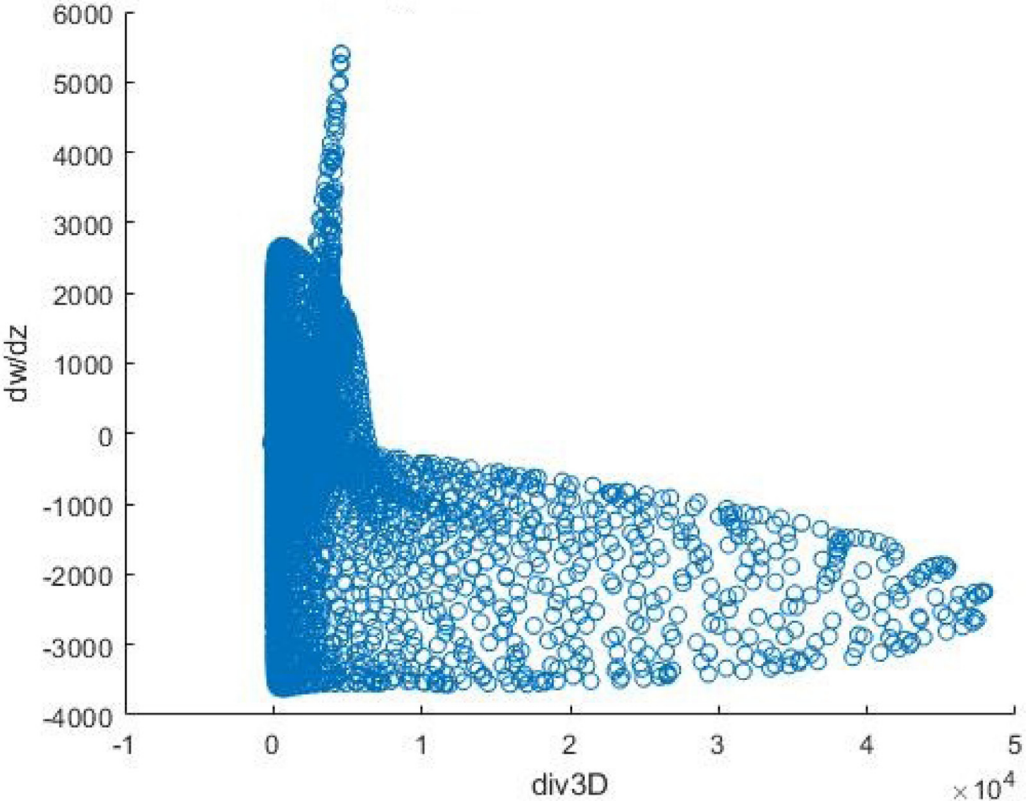

Fig. 8. $\frac{\partial u_3}{\partial x_3}$ against div_{3D} in reacting regions.

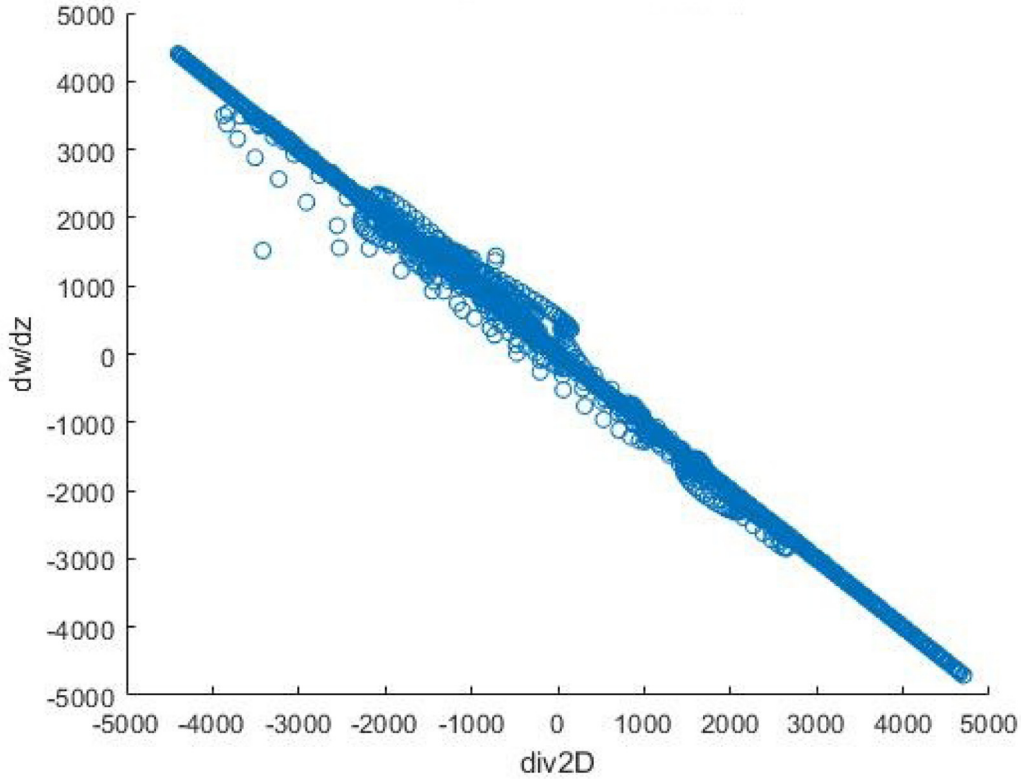

Fig. 9. $\frac{\partial u_3}{\partial x_3}$ against div_{2D} in non-reacting regions.

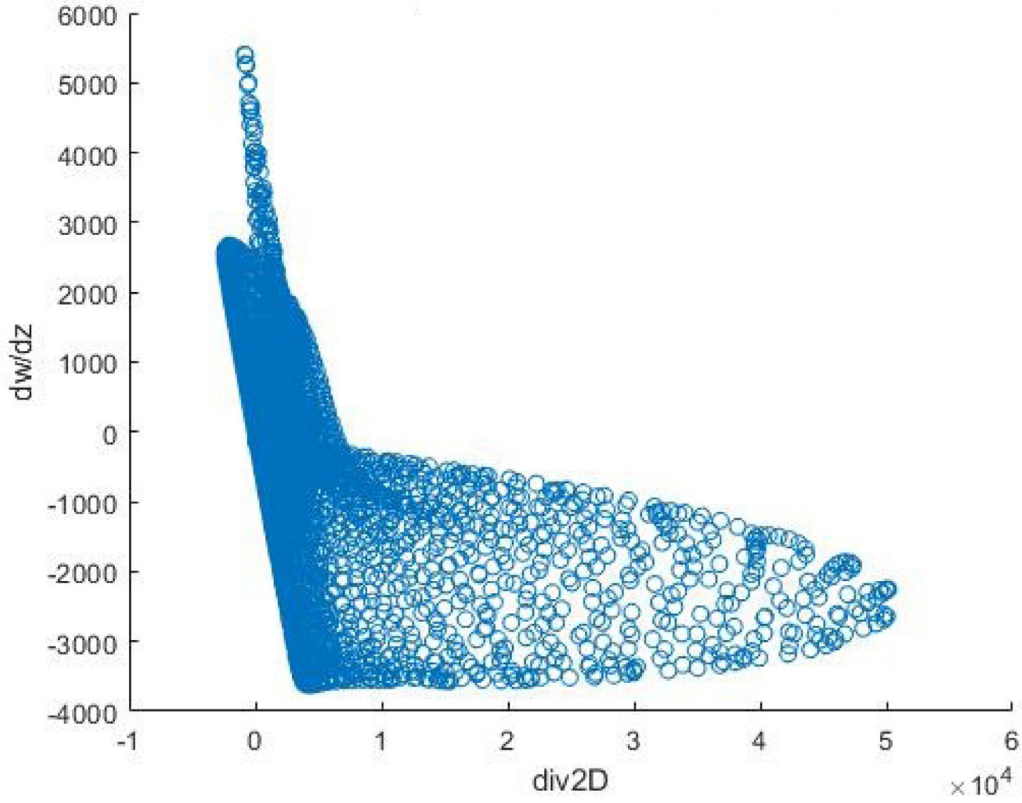

Fig. 10. $\frac{\partial u_3}{\partial x_3}$ against div_{2D} in reacting regions.

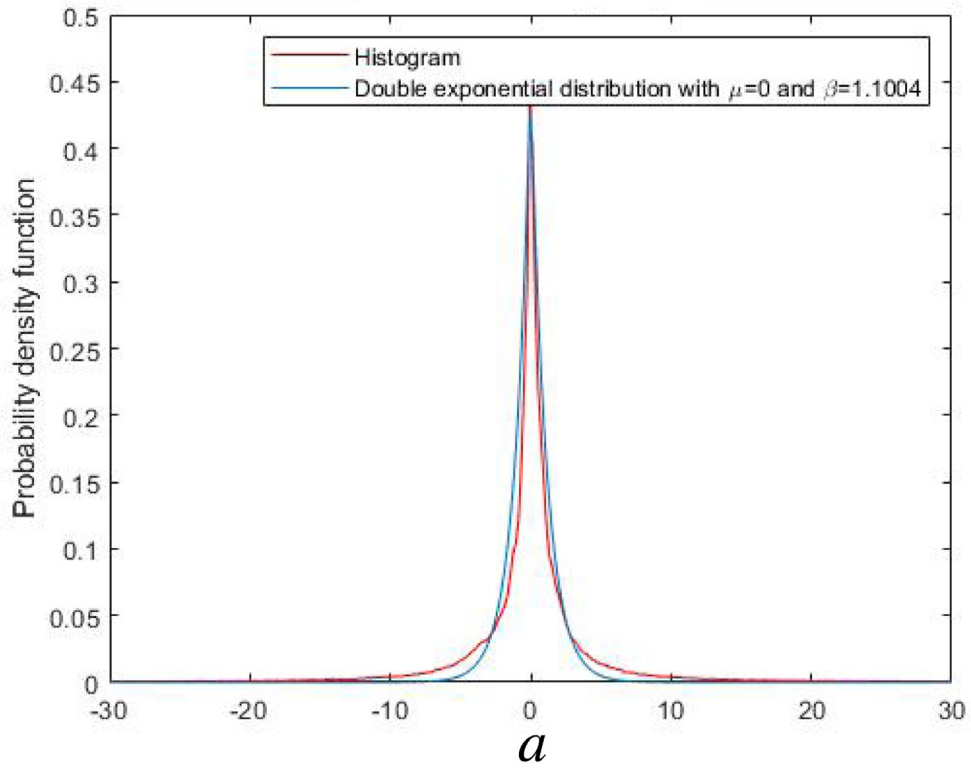

Fig. 11. Double exponential fitting (blue) of the DNS data (red) for values of the a matrix. (For interpretation of the references to colour in this figure legend, the reader is referred to the web version of this article.)

randomly generated matrices a and b such as

$$\frac{\partial u_1}{\partial x_3} = a\frac{\partial u_1}{\partial x_1} \tag{10}$$

$$\frac{\partial u_2}{\partial x_3} = b\frac{\partial u_2}{\partial x_2} \tag{11}$$

The DNS data set was used to find distributions for a and b components. A double exponential distribution is chosen, defined by its Probability Density Function (PDF) :

$$pdf(v) = \frac{1}{2\beta} exp\left(-\frac{|v-\mu|}{\beta}\right) \tag{12}$$

where v is either a or b, as appropriate. The best-fit parameters determined for both matrices were zero mean velocity, $\mu_a = \mu_b = 0$, and $\beta_a = 1$ and $\beta_b = 1.9$. The degree of fit is shown in Figs. 11 and 12. The error that we incur with this practice is expected to be small because the experimental flame is statistically two dimensional. It is difficult to quantify the resulting error without full data.

2.6. Reaction progress variable gradient approximation, $\partial c/\partial x_3$

No method for recovering $\frac{\partial c}{\partial x_3}$ has been found. Thus, our aim is to estimate the magnitude of its contribution to the tangential strain rate. First, we define the reactive contribution a_T^r to the tangential strain rate :

$$a_T^r = n_i n_j e_{ij} \tag{13}$$

The terms of a_t^r involving n_3 are compared to a_t^r. Those terms are $n_1 n_3 e_{13}$, $n_2 n_3 e_{23}$ and $n_3 n_3 e_{33}$. It is found that these are not negligible in a substantial part of the window: Fig. 13 shows this for one term, $n_3 n_3 e_{33}$ normalised by $n_3 n_3 e_{33} + a_T^r$, and a similar result is found for the other two.

Second, we note that the quantity of interest, following the work of Doan et al. [24], is the surface-averaged strain rate $\psi\left(L_s^+\right)$ for a given bandpass filtered scale L_s, as defined in Eq. (5). The divergence of c is taken as a proxy for the flame surface density by which one weights the quantity of interest. Thus, a large divergence of c means locally large surface. The definition was originally for a thin flame but can be generalised to a thick flame [5]. The fractional contribution of each scale is defined in Eq. (4). We perform a multiscale analysis with the assumption of $n_3 = 0$ to investigate the magnitude of the discrepancy in the magnitude, and location, of the peak contribution, and also in the general shape of the distribution. This approach rests on the fact that the flow is close to spatially homogenous on average in the x_3 direction, hence the assumption may nevertheless allow conclusions to be drawn.

Fig. 14 shows $\widetilde{\psi}\left(L_s^+\right)$ against the range of filtered scales using both the exact value of n_3 as well as the result of the calculation using the assumption that $n_3 = 0$. The figure shows that the assumption results in a peak which is overestimated, with underestimated L_s^+ value, but that the general shape of the distribution is comparable. The assumption will allow us to draw qualitative conclusions.

The $\frac{\partial c}{\partial x_3}$ term is involved in the analysis of the flame stretch only. Hence, as for the experimental data, the multiscale analysis will be conducted under the same assumption of $n_3 = 0$ below.

3. Experimental results

3.1. Influence of combustion on vortex stretching

The question to be addressed in this sub-heading is whether combustion modifies the vortex stretching mechanism, by refer-

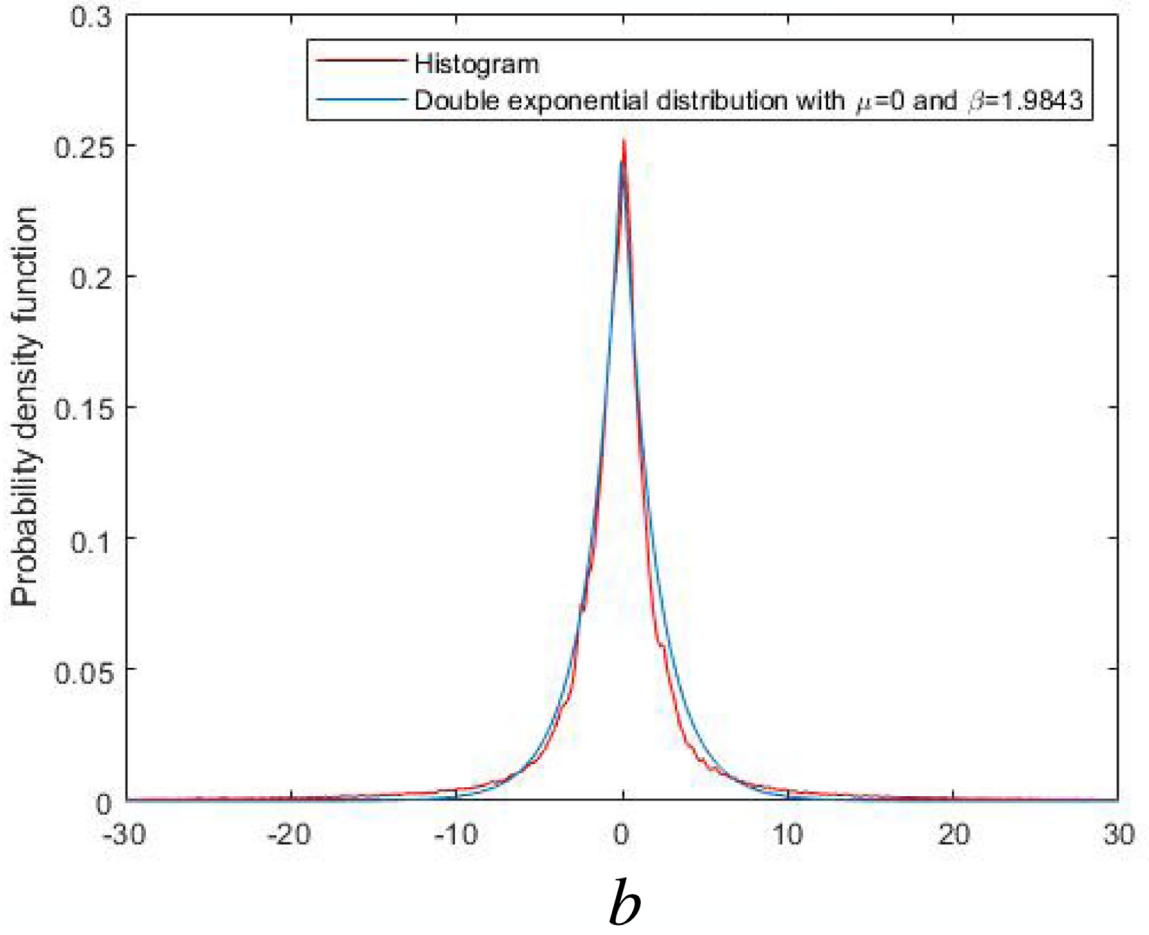

Fig. 12. Double exponential fitting (blue) of the DNS data (red) for values of the b matrix. (For interpretation of the references to colour in this figure legend, the reader is referred to the web version of this article.)

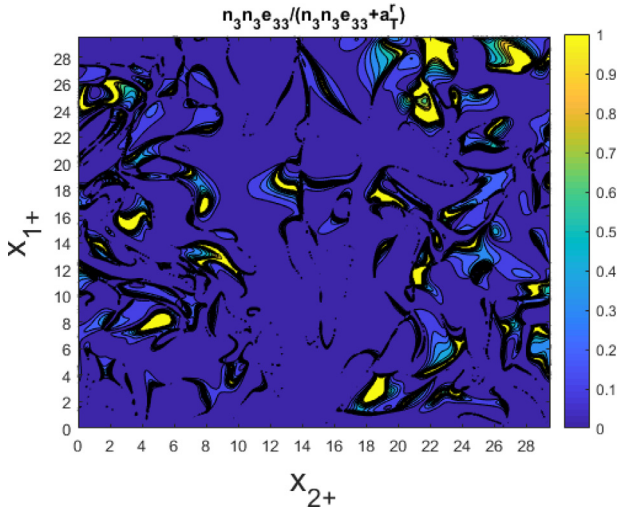

Fig. 13. Contribution of $n_3n_3e_{33}$ to the reactive part of the tangential strain rate, normalised by $n_3n_3e_{33} + a_T^r$. The numbers on ordinate and abscissa are distances normalised by δ_{th}.

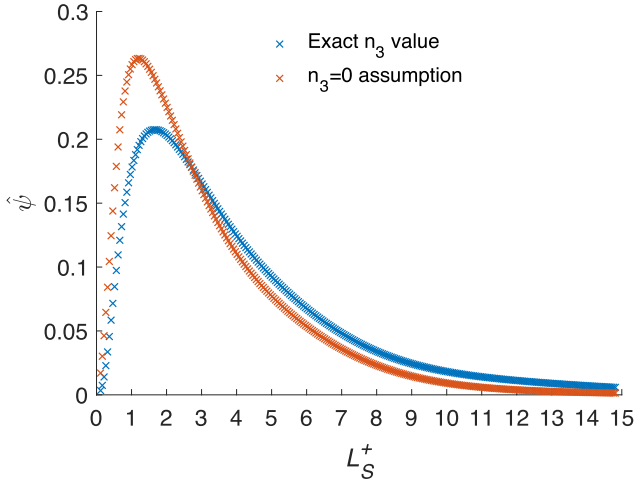

Fig. 14. Result from DNS data: surface averaged tangential strain rate, $\widehat{\psi}$, from eddies characterised by bandpass filtering scale scale L_s^+, normalised by total contribution for $u'/S_L = 2$.

ence to non-reacting flow, whereby eddies of smaller size are produced by the stretching and subsequent breaking of larger eddies. Here, this is investigated in terms of the alignment between the vorticity vector of a filtered field, $\underline{\omega}^{L_\omega}$, and the principal component of a filtered strain rate tensor, $e_{ij}^{L_s}$. Note that L_ω and L_s are independent variables and not necessarily equal. The most extensional, the most compressive, and intermediate principal components are denoted by α^{L_s}, γ^{L_s} and β^{L_s} respectively and the degree of alignment is given by the cosine of the angles, θ_i, between the vorticity vector and the principal components ($i = \alpha, \beta, \gamma$). To produce enstrophy through stretching, the vorticity has to align with

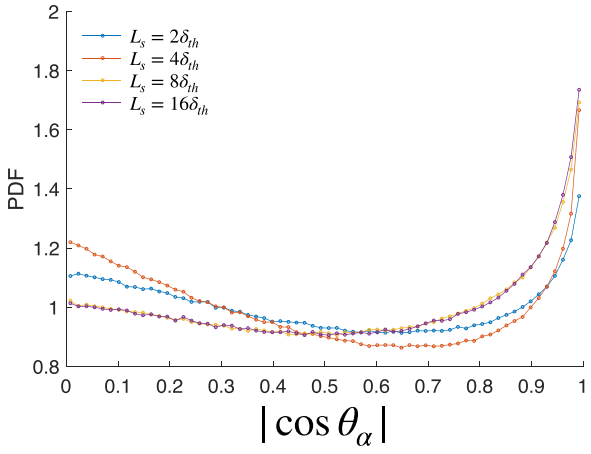

Fig. 15. Probability of alignment ($|\cos\theta_\alpha|$) between vorticity at scale $L_\omega = 4\delta_{th}$ and principal strain rate α with scale L_s ($L_s = 2\delta_{th}, 4\delta_{th}, 8\delta_{th}, 16\delta_{th}$) as parameter with $u'/s_L = 3.0$ for flame 1.

α^{L_S} or the positive part of β^{L_s}. In this work, we concentrate on the most extensional principal component. The probability function, discretised into 64 bins of width $1/64 \approx 0.015$, of $|\cos\theta_\alpha|$ for bandpass filtered fields of premixed flame with $u'/s_l = 3.0$, is shown in Fig. 15 for $L_{\omega=}4\ \delta_{th}$ and $2\delta_{th} \le L_s \le 16\delta_{th}$. The presented results are for the non-reacting regions of the flow only, *i.e.* where $|\underline{grad}\ c| < 1mm^{-1}$, although we include regions both upstream and downstream of the flame front. All figures below are the result of averaging well over 2000 images. We perform the analysis for the whole domain (which contains regions both close to the flame and further from the flame effects) to have a general view on what is happening. We anticipate the results below by stating that we observed similar behaviour to that for non-reacting turbulence so there was no strong effect of the flame on this vortex stretching mechanism (as could have been possible, for example, in the downstream region after the flame dissipated some turbulence).

The uncertainties in the results below, based on estimates of the vorticity and rate of strain, stem from uncertainty in the measurement of velocity by a PIV and the corresponding error in the estimation of velocity gradients due to the finite spatial resolution of the PIV and the implied spatial averaging (in these experiments, we expect errors from out-of-plane convection and gradients on the results to be small in this flow because it is two dimensional in the mean). Worth et al. [35] quantified these sources by reference to DNS calculations in homogeneous isotropic turbulence. They advise a spatial resolution (to minimise loss of fine scale information) of the order of $2-3\eta$, as used here, to resolve fine scale features and they report levels of gradient uncertainty at around 20%. In an experiment closer to that reported in this work, [17] and [18] also indicate that a spatial resolution of 3η results in estimates of gradients that do not suffer from excessive smoothing. Steinberg and Driscoll [17] report that for ω_i and e_{ij}, the maximum r.m.s. error is be expected as less than 7\%. The uncertainty in the estimation of $|\cos\theta_i|$ is related to those in ω_i and e_{ij} and we thus estimate these quantities to be around 15 percent. The additional errors that arise during the computation of the strain-rate on the flame, a_T, they estimate as less than 10 per cent.

Fig. 15 shows that, for the most extensional principal component, α, the results are qualitatively consistent with [24] in that indeed vorticity is more likely to be aligned with the most extensive α strain direction, at all investigated scales of L_s, from 2 to 16 δ_{th}, although here there is also evidence of prevalence at $|\cos\theta_\alpha| = 0$. However, we are unable to confirm their observation that such preferential alignment disappears abruptly below $L_s = 3\ \delta_{th}$ because we present results for a vortical structure of $L_\omega = 4\delta_{th}$

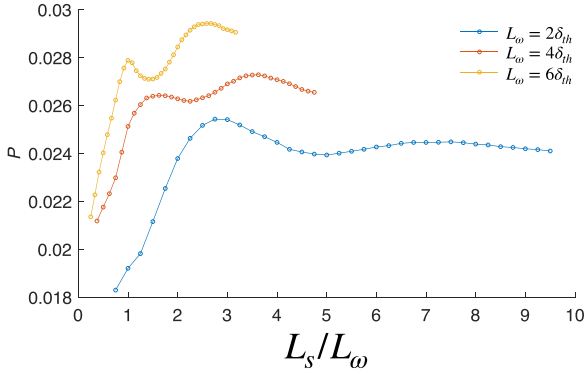

Fig. 16. Probability of alignment ($63/64 \le |\cos\theta_\alpha| \le 1$) between vorticity at scale L_ω and principal strain rate α at scale L_s with the magnitude of L_ω ($L_\omega = 2\delta_{th}, 4\delta_{th}, 6\delta_{th}$) as parameter for flame 1.

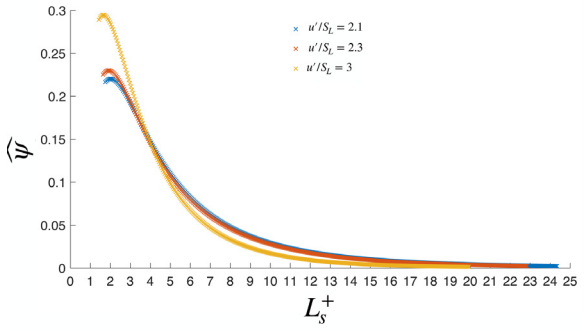

Fig. 17. Surface averaged tangential strain rate, $\psi(L_s^+)$, from eddies of scale L_s^+, normalised by total contribution, ψ_{int}: $\widehat{\psi} = \psi(L_s^+)/\psi_{int}$ with the assumption of \$n_3 = 0\$. Flames 1, 2, 3 averaged over 2816 frames.

only while [24] were able to consider $L_\omega = \delta_{th}$. This is a limitation of the experimental apparatus where we cannot have as high a resolution as in DNS and we therefore cannot assess the impact of these smaller scales of turbulence. However, from past studies from DNS [24], we see that the most important scales of turbulence are generally larger than the flame thermal thickness. So, the analysis that we can obtain from these data is still meaningful.

Fig. 16, for flame 1 in Table 2, quantifies which eddy length scales L_s impart the most stretch on vortical structures of scale $L_\omega = 2\delta_{th}, 4\delta_{th}$ and $6\delta_{th}$ by presenting the probability, P, for $63/64 \le |\cos\theta_\alpha| \le 1$ with the magnitude of L_ω as parameter[2]. The figure shows that there is, consistently, a broad peak between 2 and 4 times the considered value of $L_\omega\delta_{th}$ (to avoid ambiguity, this means that the peak for $L_\omega = 6\delta_{th}$, which is at about $2.6L_\omega$, corresponds to $L_s \approx 2.6 \cdot 6 \cdot \delta_{th}$) which accords with the expectation from the non-reacting work of [25]. Of greater direct relevance is that there is also qualitative agreement with the findings of [24] in premixed flames, although they were able to resolve down to $L_\omega = \delta_{th}$ which we are not able to with this data set.

3.2. Multiscale analysis of tangential strain rate

We estimate, as above, the normalised surface-averaged tangential strain rate, $\widehat{\psi}(L_s^+)$, from eddies of normalised bandpass filtered scale L_s^+, Eq. (4).

Fig. 17 shows the variation of the fractional contribution $\widehat{\psi} = \psi(L_s^+)/\psi_{int}$ with L_s^+ for flames 1, 2 and 3. The result of Fig. 14 does not permit the determination of the location of the peak contribu-

[2] Note that the probabilities are low in this figure because these events are conditional on occurring in the narrow window $63/64 \le |\cos\theta_\alpha| \le 1$

Table 4
L_R [20] and Gibson cutoff scales .

Flame	L_R/δ_{th}	L_G/δ_{th}
1	1.8	3.3
2	2.2	8.7
3	0.9	12.1

tion with confidence, other than to say that it is above $L_s^+ \approx 2$ in our measurements and, using figure 14 as a guide, may be at $L_s^+ \approx 3$ or 4. Note that the slight evidence of the maximum in the figure is not due to curve fitting, but due to measurement: indeed, more convincing maxima are to be found in individual frames. Also, the differences between the three flames in terms of Lewis number, which is arguably the main distinguishing parameter between these, and to a lesser extent the laminar burning velocity, does not result in any noticeable change in the shape of the dependence. It is worth noting that length scales of these magnitudes are similar to the inner cut-off scale estimates based on fractal analysis of flame surface density [36–48] and scalar dissipation rate closures [49].

For flames with u'/s_L comparable to those here, Doan et al. [24] found peaks between $5 \leq L_s^+ \leq 10$ and, for flames with higher turbulence intensity, found that the peak value is shifted towards values of L_s^+ of about 2 to 3, which thus establishes a range of values comparable to the estimates here. Furthermore, the rapid decrease in contributions from eddies of sizes larger than that associated with the peak in the experiments has some parallel with the higher turbulence intensity flames of [24] up to $L_s^+ \approx 6$. Nevertheless, the results presented here have been made assuming that $n_3 = 0$ and therefore we cannot reliably estimate the relative contribution of eddies smaller than, say, $2\delta_{th}$ on the total tangential strain rate. A crude estimate, on the basis of the magnitude of the correction to figure 17 implied by figure 14, is that it is of the order of about 1/5th, which is larger than the value of 10 per cent quoted by Doan et al. [24]. In summary, the current experiments suggest that the range of eddies which have a substantial effect on flame straining is comparable to the range found by Doan, namely $3 \leq L_s^+ \leq 17$.

Estimates in the literature for the smallest length scales are, as mentioned earlier, L_R [20]

$$(L_R/\delta_{th}) = \left(u'/s_L\right)^{-3/4} (\Lambda/\delta_{th})^{1/4} \tag{14}$$

and the Gibson scale L_G. Values for these length scales, normalised by δ_{th}, are given in Table 4 (where we estimate $\epsilon = 15\nu u'^2/\lambda^2$). These values are higher than the corresponding values in [24], once again presumably because of the higher turbulent Reynolds number in the experiments. The work of Gulder and Smallwood [50] provides some support for this suggestion from examination of data from experimental and direct numerical simulation. They found that an inner cut-off scale of flame surface wrinkling varied as Ka^{β}, where Ka is the Karlovitz number, with β of the order of -1/2 or -1/3. This therefore also suggests a decrease of this cut-off scale with increasing turbulence intensity. However, particularly given the uncertainty here in the estimate of ϵ, the range of eddies having weak influence in straining flame needs further examination.

The broader conclusion of [24] stands, however, in that it is turbulent structures larger than about $2\delta_{th}$ which have substantial effect and thus it may be unnecessary to resolve smaller scales, at least in the context of flame stretch. Here it is recalled that the bandpass filter has a sharper roll-off at scales smaller than the 'centre' value than at larger scales. Thus the results here are, as noted by Doan et al. [24], conservative estimates and the practical implication is that, in large eddy simulations (LES), the effort required to resolve scales as small as δ_{th} may be unnecessary. This is a tentative conclusion which certainly deserves further experimental study over a wider range of parameter space in the Borghi-Peters diagram, with instrumentation that permits resolution of $L_\omega = \delta_{th}$ and is able to resolve the full rate of strain tensor.

4. Conclusions

We have applied bandpass multiscale analysis to three sets of experimental measurements of premixed, turbulent, V-flames straddling the border between corrugated flamelets and thin reaction zone in the Borghi-Peters diagram. The turbulent Reynolds number investigated here is a factor of about four larger than that examined previously using DNS, while the ratio of characteristic turbulent velocity to laminar flame speed, u'/s_L, is between 2 and 3 while the DNS studies extended this to about 11. For each flame there is a comprehensive data set in one plane only. Approximations for the missing out-of-plane derivatives have been constructed, aided by the flow being close to two - dimensional on average, and by recourse to comparisons with a DNS calculation of a similar flow. For $\partial u_3/\partial x_3$ we have used the approximation $-\partial u_1/\partial x_1 - \partial u_2/\partial x_2$ in non-reacting regions, and $\partial u_3/\partial x_3 = 0$ where reaction takes place. For the out-of-measurement-plane gradients of velocity, we have used exponential distributions curve-fitted to the results from the DNS calculation for the probability functions of $\partial u_1/\partial x_3$ and $\partial u_2/\partial x_3$. For the calculation of the reactive strain rate, we have used the approximation that $n_3 = 0$, once again establishing the effect of doing so by recourse to the DNS data.

This work quantifies two aspects of turbulence-flame interaction. The first aspect is that of the flame interaction of eddies of size L_s on the turbulence as found by the statistics of the alignment of vorticity with strain rate. We find that vortical eddies with scale about $L_\omega = 2\delta_{th}$ are stretched by L_s structures which are larger than about 2 L_ω, with this factor broadly true also for vortical eddies of scales $L_\omega = 4\delta_{th}$ and $L_\omega = 6\delta_{th}$. Within the limitations of the data set, these findings are comparable to those of [24] in reacting and [25] in non-reacting flows, although these authors were able to investigate resolutions down to $L_\omega = \delta_{th}$. Doan et al. [24] concluded that the premixed flame had negligible influence on the vortex stretching mechanism and our results here are consistent with this finding.

The second aspect of turbulence-flame interaction examined is that of flame surface averaged tangential strain rate imparted by eddies. Eddies with length scales L_s estimated to be about 3 to $4\delta_{th}$ have the strongest individual contribution but may nevertheless contribute only about 1/5th of the total tangential strain rate. This is larger than the 10% that has been reported by Doan et al. [24] based on analysis of DNS predictions of premixed flames at turbulent Reynolds numbers up to 110. Eddies with length scale L_s larger than about $20\delta_{th}$ contribute a negligible amount to the total tangential strain rate. The latter conclusion is also in accordance with that of [24].

In the context of large eddy simulations (LES) of premixed combustion, these results are preliminary experimental evidence supporting the suggestion made in [24] that resolving turbulence scales down to a few multiples of δ_{th} might be adequate to capture much of the flame *straining* caused by turbulence.[3] Further experimentation is required for a broader area in the Borghi-Peters diagram, with instruments which can resolve scales close to the flame thickness and permit estimation of the full rate of strain tensor without the approximations used here. The aim of further work is

[3] However, this is not to deny the importance of smaller scales which, as reviewed by [51], may well affect the inner flame structure.

to establish the range of conditions flames that can be calculated adequately by LES equations without additional modelling to describe sub-grid scale flame stretching. We have found no evidence that the Lewis number up to about 1.8 has an observable effect, but this may reflect the inability of the current instruments to resolve vortical structures down to $L_\omega = \delta_{th}$. This is a topical question in view of the possible widespread adoption of hydrogen, and its related vector fuels, in future combustion systems.

Declaration of Competing Interest

The authors declare that they have no known competing financial interests or personal relationships that could have appeared to influence the work reported in this paper.

Acknowledgements

We thank Dr Tom Dunstan for the use of the DNS data that he calculated. Dr Antonis Sergis helped us with the management of the archiving of the large experimental data set.

References

[1] K. Bray, The interaction between turbulence and combustion, Symp. (Int.) Combust. 17 (1) (1979) 223–233.
[2] K. Bray, The challenge of turbulent combustion, Symp. (Int.) Combust. 26 (1) (1996) 1–26.
[3] S.M. Candel, T.J. Poinsot, Flame stretch and the balance equation for the flame area, Combust. Sci. Technol. 70 (1–3) (1990) 1–15.
[4] N. Peters, Turbulent combustion, Cambridge University Press, Cambridge, 2000.
[5] D. Veynante, L. Vervisch, Turbulent combustion modeling, Prog. Energy Combust. Sci. (2002) 74.
[6] E.R. Hawkes, R.S. Cant, Implications of a flame surface density approach to large eddy simulation of premixed turbulent combustion, Combust. Flame 126 (01) (2001) 1617–1629.
[7] N. Chakraborty, M. Klein, R.S. Cant, Stretch rate effects on displacement speed in turbulent premixed flame kernels in the thin reaction zones regime, Proc. Combust. Inst. 31 (1) (2007) 1385–1392.
[8] S. Ruan, N. Swaminathan, Y. Mizobuchi, Investigation of flame stretch in turbulent lifted jet flame, Combust. Sci. Technol. 186 (3) (2014) 243–272.
[9] C. Dopazo, L. Cifuentes, J. Martin, C. Jiménez, Strain rates normal to approaching isoscalar surfaces in a turbulent premixed flame, Combust. Flame 162 (5) (2015) 1729–1736.
[10] O. Colin, F. Ducros, D. Veynante, T. Poinsot, A thickened flame model for large eddy simulations of turbulent premixed combustion, Phys. Fluids 12 (7) (2000) 1843–1863.
[11] F. Charlette, C. Meneveau, D. Veynante, A power-law flame wrinkling model for LES of premixed turbulent combustion part I: non-dynamic formulation and initial test, Combust. Flame 131 (02) (2002) 159–180.
[12] H. Pitsch, Large-Eddy simulation of turbulent combustion, Annu. Rev. Fluid Mech. 38 (1) (2006) 453–482.
[13] H. Kolla, N. Swaminathan, Strained flamelets for turbulent premixed flames, I: formulation and planar flame results, Combust. Flame 157 (5) (2010) 943–954.
[14] C. Meneveau, T. Poinsot, Stretching and quenching of flamelets in premixed turbulent combustion, Combust. Flame 86 (4) (1991) 311–332.
[15] S. Bougrine, S. Richard, O. Colin, D. Veynante, Fuel composition effects on flame stretch in turbulent premixed combustion: numerical analysis of flame-Vortex interaction and formulation of a new efficiency function, Flow, Turbul. Combust. 93 (2) (2014) 259–281.
[16] F. Thiesset, G. Maurice, F. Halter, N. Mazellier, C. Chauveau, Flame-vortex interaction : effect of residence time and formulation of a new efficiency function, Proc. Combust. Inst. 000 (2015) 1–9.
[17] A.M. Steinberg, J.F. Driscoll, Straining and wrinkling processes during turbulence-premixed flame interaction measured using temporally-resolved diagnostics, Combust. Flame 156 (12) (2009) 2285–2306.
[18] A.M. Steinberg, J.F. Driscoll, Stretch-rate relationships for turbulent premixed combustion LES subgrid models measured using temporally resolved diagnostics, Combust. Flame 157 (7) (2010) 1422–1435.
[19] T. Poinsot, D. Veynante, S.M. Candel, Quenching processes and premixed turbulent combustion diagrams, J. Fluid Mech. 228 (1991) 561–606.
[20] W.L. Roberts, J.F. Driscoll, M.C. Drake, L.P. Goss, Images of the quenching of a flame by a vortexto quantify regimes of turbulent combustion, Combust. Flame 94 (1) (1993) 58–69.
[21] A.N. Lipatnikov, S. Nishiki, T. Hasegawa, A direct numerical simulation study of vorticity transformation in weakly turbulent premixed flames, Phys. Fluids 26 (10) (2014) 105104.
[22] Y. Nada, M. Tanahashi, T. Miyauchi, Effect of turbulence characteristics on local flame structure of H2-air premixed flames, J. Turbul. 5 (2004) 37–41.
[23] B. Yenerdag, N. Fukushima, M. Shimura, M. Tanahashi, T. Miyauchi, Turbulence-flame interaction and fractal characteristics of H2-air premixed flame under pressure rising condition, Proc. Combust. Inst. 35 (2) (2015) 1277–1285.
[24] N. Doan, N. Swaminathan, N. Chakraborty, Multiscale analysis of turbulence-flame interaction in premixed flames, Proc. Combust. Inst. 36 (2) (2017) 1929–1935.
[25] T. Leung, N. Swaminathan, P.A. Davidson, Geometry and interaction of structures in homogeneous isotropic turbulence, J. Fluid Mech. 710 (2012) 453–481.
[26] T. Sponfeldner, I. Boxx, F. Beyrau, Y. Hardalupas, W. Meier, A.M.K.P. Taylor, On the alignment of fluid-dynamic principal strain-rates with the 3D flamelet-normal in a premixed turbulent v-flame, Proc. Combust. Inst. 35 (2) (2015) 1269–1276, doi:10.1016/j.proci.2014.06.082.
[27] T. Sponfeldner, The effect of fractal grid generated turbulence on the structure of premixed flames, Imperial College London, London U.K., 2014 Ph.D. thesis.
[28] D. Hurst, J.C. Vassilicos, Scalings and decay of fractal-generated turbulence, Phys. Fluids 19 (3) (2007) 035103. Publisher: American Institute of Physics
[29] N. Soulopoulos, J. Kerl, T. Sponfeldner, F. Beyrau, Y. Hardalupas, A.M.K.P. Taylor, J.C. Vassilicos, Turbulent premixed flames on fractal-grid-generated turbulence, Fluid Dyn. Res. 45 (6) (2013) 061404.
[30] F. Halter, C. Chauveau, I. Gokalp, D. Veynante, Analysis of flame surface density measurements in turbulent premixed combustion, Combust. Flame 156 (3) (2009) 657–664.
[31] D. Veynante, G. Lodato, P. Domingo, L. Vervisch, E.R. Hawkes, Estimation of three-dimensional flame surface densities from planar images in turbulent premixed combustion, Exp. Fluids 49 (1) (2010) 267–278.
[32] E.R. Hawkes, R. Sankaran, J.H. Chen, Estimates of the three-dimensional flame surface density and every term in its transport equation from two-dimensional measurements, Proc. Combust. Inst. 33 (1) (2011) 1447–1454.
[33] T.D. Dunstan, N. Swaminathan, K.N.C. Bray, Influence of flame geometry on turbulent premixed flame propagation: a DNS investigation, J. Fluid Mech. 709 (2012) 191–222. Publisher: Cambridge University Press
[34] N. Swaminathan, R.W. Bilger, G.R. Ruetsch, Interdependence of the instantaneous flame front structure and the overall scalar flux in turbulent premixed flames, Combust. Sci. Technol. 128 (1997) 73–97.
[35] N.A. Worth, T.B. Nickels, N. Swaminathan, A tomographic PIV resolution study based on homogeneous isotropic turbulence DNS data, Exp. Fluids 49 (3) (2010) 637–656.
[36] F.C. Gouldin, An application of fractals to modeling premixed turbulent flames, Combust. Flame 68 (3) (1987) 249–266.
[37] F.C. Gouldin, S.M. Hilton, T. Lamb, Experimental evaluation of the fractal geometry of flamelets, Symp. (Int.) Combust. 22 (1) (1989) 541–550.
[38] F.C. Gouldin, K.N.C. Bray, J.-Y. Chen, Chemical closure model for fractal flamelets, Combust. Flame 77 (3–4) (1989) 241–259.
[39] G.L. North, D.A. Santavicca, The fractal nature of premixed turbulent flames, Combust. Sci. Technol. 72 (4–6) (1990) 215–232.
[40] O.L. Gulder, Turbulent premixed combustion modelling using fractal geometry, Symp. (Int.) Combust. 23 (1991) 835–842.
[41] N. Peters, Turbulent combustion, Cambridge University Press, Cambridge, 2000.
[42] E. Giacomazzi, C. Bruno, B. Favini, Fractal modelling of turbulent combustion, Combust. Theory Model. 4 (4) (2000) 391–412.
[43] E. Giacomazzi, V. Battaglia, C. Bruno, The coupling of turbulence and chemistry in a premixed bluff-body flame as studied by LES, Combust. Flame 138 (2004) 320–335.
[44] N.K. Aluri, S.P.R. Muppala, F. Dinkelacker, Substantiating a fractal-based algebraic reaction closure of premixed turbulent combustion for high pressure and the lewis number effects, Combust. Flame 145 (4) (2006) 663–674.
[45] E. Giacomazzi, F.R. Picchia, N. Arcidiacono, D. Cecere, F. Donato, B. Favini, Unsteady simulation of a CO/H2/N2/air turbulent non-premixed flame, Combust. Theory Model. 12 (6) (2008) 1125–1152.
[46] E.R. Hawkes, O. Chatakonda, H. Kolla, A.R. Kerstein, J.H. Chen, A petascale direct numerical simulation study of the modelling of flame wrinkling for large-eddy simulations in intense turbulence, Combust. Flame 159 (8) (2012) 2690–2703.
[47] F. Cavallo Marincola, T. Ma, A.M. Kempf, Large eddy simulations of the Darmstadt turbulent stratified flame series, Proc. Combust. Inst. 34 (1) (2013) 1307–1315.
[48] R. Keppeler, E. Tangermann, U. Allaudin, M. Pfitzner, LES of low to high turbulent combustion in an elevated pressure environment flow, Turbul. Combust. 92 (3) (2014) 767–802.
[49] Y. Gao, N. Chakraborty, N. Swaminathan, Algebraic closure of scalar dissipation rate for large eddy simulations of turbulent premixed combustion, Combust. Sci. Technol. 186 (10–11) (2014) 1309–1337.
[50] O.L. Gulder, G.J. Smallwood, Inner cutoff scale of flame surface wrinkling in turbulent premixed flame, Combust. Flame 103 (1–2) (1995) 107–114.
[51] J.F. Driscoll, J.H. Chen, A.W. Skiba, C.D. Carter, E.R. Hawkes, H. Wang, Premixed flames subjected to extreme turbulence: some questions and recent answers, Prog. Energy Combust. Sci. 76 (2020) 100802.